

Mapping Cell-Matrix Stresses during Stretch Reveals Inelastic Reorganization of the Cytoskeleton

Núria Gavara,* Pere Roca-Cusachs,* Raimon Sunyer,* Ramon Farré,*[†] and Daniel Navajas*^{†‡}

*Unitat de Biofísica i Bioenginyeria, Facultat de Medicina, Universitat de Barcelona-IDIBAPS, Barcelona, Spain; [†]Ciber Enfermedades Respiratorias, Bunyola, Spain; and [‡]Institut de Bioenginyeria de Catalunya, Barcelona, Spain

ABSTRACT The mechanical properties of the living cell are intimately related to cell signaling biology through cytoskeletal tension. The tension borne by the cytoskeleton (CSK) is in part generated internally by the actomyosin machinery and externally by stretch. Here we studied how cytoskeletal tension is modified during stretch and the tensional changes undergone by the sites of cell-matrix interaction. To this end we developed a novel technique to map cell-matrix stresses during application of stretch. We found that cell-matrix stresses increased with imposition of stretch but dropped below baseline levels on stretch release. Inhibition of the actomyosin machinery resulted in a larger relative increase in CSK tension with stretch and in a smaller drop in tension after stretch release. Cell-matrix stress maps showed that the loci of cell adhesion initially bearing greater stress also exhibited larger drops in traction forces after stretch removal. Our results suggest that stretch partially disrupts the actin-myosin apparatus and the cytoskeletal structures that support the largest CSK tension. These findings indicate that cells use the mechanical energy injected by stretch to rapidly reorganize their structure and redistribute tension.

INTRODUCTION

Adherent cells such as those found in the lungs, heart, or muscle are subjected to substantial stretch. Stretch is in turn known to regulate fundamental cellular functions including growth, spreading, migration, mechanotransduction, differentiation, apoptosis, and protein synthesis (1–5). Cellular response to stretch and the transmission of applied stresses through the cell are largely determined by its cytoskeleton (CSK), a tensed network of crosslinked semiflexible polymers (4,6,7). The tension borne by these polymers, known as cell prestress, is generated in part by the actomyosin machinery (6). In response to contractile agonists, for example, the cytoskeleton undergoes structural and biochemical changes including actin polymerization, formation of stress fibers, and phosphorylation of myosin light chain (MLC) that ultimately lead to increased CSK tension (8,9). CSK tension can also be externally regulated by stretch. When stretch is applied to the cell, the CSK deforms, filaments reorient, and stress transmission through the network is altered (4,10–15). However, the way in which CSK tension is modified during stretch and the identification of the specific loci of cell-matrix interactions that undergo tensional changes remains a major open question.

In vitro studies in crosslinked networks of semiflexible biopolymers predict that as the cell is stretched, nonlinear entropic elasticity of single filaments will lead to a steep increase in CSK tension (16–18). A similar outcome can be derived from models of stress-supported structures such as

tensegrity (4,6,10). Such predictions are consistent with studies in living cells that show stress-induced increases in cell stiffness (19–23). A very different scenario, however, is the one predicted by the soft glassy cell model. Soft glassy materials such as colloids, foams and pastes are known to soften in response to stretch, and such behavior has also been observed in the living cell (24).

Due mainly to technical limitations, few data are available on the effect of stretch on cell mechanical stress. Cell stress has been studied with traction microscopy (TM) (25,26), which maps the traction forces exerted by a cell adhered onto the surface of an elastic gel with embedded fluorescent microbeads. TM first maps cell-induced gel deformations by tracking the displacement of the microbeads through cross-correlation of epifluorescence microscopy images (27). The gel deformation field is then used to compute the traction field exerted by the adhered cell. Although the effect of different stimuli on cell traction forces has been extensively studied under static conditions by TM (25,27,28), current implementation of this technique is not suited to probing cell traction during stretch. We recently developed a device mounted on an inverted fluorescence microscope that enables the stretching of cells attached to a flexible membrane that is uniformly and equibiaxially distended by a vacuum source (20). We report a novel TM technique to map cell-matrix stresses during application of stretch. The technique is based on combining traction microscopy with the cell stretching device. Cell stretching is produced by distending a collagen gel attached to a flexible membrane with a vacuum-driven device mounted on an epifluorescence microscope. We improved the conventional TM setup and generalized common computational algorithms to map traction forces under uniform and equibiaxial cell stretching.

Submitted October 22, 2007, and accepted for publication February 28, 2008.

Address reprint requests to Prof. Daniel Navajas, Unitat Biofísica i Bioenginyeria, Facultat Medicina, Casanova 143 08036, Barcelona, Spain. Tel.: 34-93-402-4515; Fax: 34-93-403-5278; E-mail: dnavajas@ub.edu.

Editor: Gerard Marriott.

Using the new TM technique we found that stresses exerted by adhered cells increased with imposition of stretch but dropped below baseline levels on stretch release. When the actomyosin machinery was inhibited, the relative increase in CSK tension with stretch was larger than in control cells and the drop in cell-matrix stress after stretch release was smaller. The analysis of stress maps before and after stretch application showed that the cell-matrix interactions exhibiting bigger drops in stress were those that bore larger stresses before stretch. Therefore, our results suggest that stretch partially disrupts the actomyosin apparatus and the cellular structures that support the largest initial CSK tension.

MATERIALS AND METHODS

Cell culture and staining

A549 human alveolar epithelial cells were obtained from ATCC (Manassas, VA). Cells were cultured in RPMI 1640 medium supplemented with 1 mM L-glutamine, 100 U/ml penicillin, 100 mg/ml streptomycin, and 2 μ g/ml amphotericin B (all from GIBCO, Gaithersburg, MD), 10% inactivated fetal calf serum (Biological Industries, Kibbutz Beit Haemek, Israel) and buffered with HEPES (Sigma, St. Louis, MO). For traction microscopy experiments, cells were plated sparsely on collagen gels (3×10^4 cells/gel) attached to flexible-bottomed culture wells (35 mm diameter; Bioflex, Flexcell International, PA). The culture medium was replaced by serum-free medium before experiments. For measurements with MLCK inhibition, cells were incubated with 10 μ M ML7 (Sigma) 30 min before stretching. The inhibitor was not washed out during the stretching maneuver. Actin staining experiments were done on collagen I-coated flexible-bottomed culture wells at confluence. To localize F-actin and G-actin, cells were fixed with 3.7% formaldehyde, permeabilized with 0.1% Triton X-100, and stained with Phalloidin-TRITC (Sigma) and Alexa Fluor 488 DNase I conjugate (Molecular Probes, Eugene, OR).

Technique to map cell-matrix stresses during stretch

Flexible-bottomed culture wells were initially coated with collagen (4 μ g/cm²) by flushing 500 ml of 0.3 mg/ml type I collagen (Upstate, Lake Placid, NY) diluted in PBS into the well and air dried. The wells were then rinsed with PBS and dried again and kept at 4°C. For TM experiments, type I collagen (1.45 mg/ml) containing fluorescent microbeads (0.2 μ m diameter) (Molecular Probes) was jellified onto the collagen-coated well membrane. Resulting gels were \sim 1 mm thick. After gel polymerization and before cell culture, collagen gels were stretched several times to assess gel-membrane attachment. We discarded gels that did not remain attached to the bottom of the well after this process. Discarded gels detached from the membrane and floated but did not break or disassemble.

To stretch the gels, we adapted a previously described stretching device, based on applying vacuum underneath a flexible-bottomed well (20) (Fig. 1) coupled to an inverted microscope (Eclipse TE2000, Nikon, Japan). A cylindrical loading post was located beneath the well to obtain equibiaxial and uniform strains in the central region of the substrate. The rising and falling times of the applied pressure step were modulated by a resistor-capacitor pneumatic filter inserted between the vacuum source and the sample. This device exhibits a linear relationship between the applied vacuum pressure and the resulting membrane stretch that is directly applied to the bottom surface of the attached gel (20). When the gel was stretched, its lateral surface remained attached to the walls of the well. As a result, the top of the gel was the only free surface, and the deformation experienced at the top was similar to that of the bottom of the gel. Owing to volume conservation, the gel became slightly thinner in the central region distant from the walls of the well.

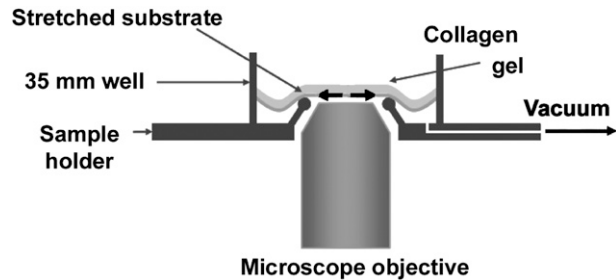


FIGURE 1 Stretching device. Collagen gels with embedded fluorescent microbeads were jellified on flexible-bottomed wells. The wells were positioned on a sample holder based on a hollow cylindrical loading-post concentric with the objective of the epi-fluorescence microscope. The application of a negative pressure underneath the annular outer region of the sample resulted in a homogeneous and equibiaxial strain of the central area.

Nevertheless, the change in gel thickness along the gel's diameter was too small to be observable in the area covered by our fluorescence images (see Fig. S1 in Supplementary Material, [Data S1](#)).

Measurement of Young's modulus of the gels

The Young's modulus (E) of collagen gels subjected to different strain levels was measured with atomic force microscopy (AFM) as described previously (29). Measurements were taken using a pyramidal-tip cantilever (Mikromasch, Estonia) with nominal spring constant $k = 0.01$ N/m. The spring constant of the cantilever was calibrated by the thermal fluctuations method in water (30). Force-displacement curves (maximal indentation depth \sim 1.5 μ m) were done at 1 Hz on five distant regions for each gel sample. Stretch was progressively increased and E was measured for each strain level. Stretch was released before moving to a different gel region, resulting in five different stretching cycles per gel. E was computed from the force-displacement curves by fitting the pyramidal contact model using nonlinear least squares regression (31). The average E measured in the gels for each stretch configuration was used for computing cell traction forces from bead displacement measurements.

Experimental protocols

Experiments started by acquiring a bright field (BF) image of a selected isolated cell cultured on a collagen gel (Fig. 2). Next, the apical surface of the gel was focused and a fluorescence image of the microbeads was acquired. The gel was stretched and the gel region studied was visually repositioned in the field of view of the microscope and refocused using bright large fluorescent spots located on the surface of the gel as a reference (see Fig. S1 in [Data S1](#)). Accurate repositioning was subsequently done by image correlation algorithms (see data processing). After 2 min of stretch application BF and fluorescence images of the cell and microbeads, respectively, were recorded. Stretch was released and 2 min later, the sample was repositioned again and new BF and fluorescence images were acquired. Subsequently, the cells were removed from the gel by exposure to trypsin, and fluorescence images were recorded to determine the position of the beads in the cell-free strained and unstrained gel. These two final fluorescence images were used as reference images (RIs) for the computation of traction forces. Finally the stretch-unstretch maneuver in the cell-free gel was repeated, together with fluorescence imaging, to assess stretch repeatability and reversibility.

Microscopy

Imaging was done using long working distance 20 \times (TM experiments) or 10 \times (actin staining experiments) objectives and an inverted fluorescence microscope (Eclipse TE2000, Nikon, Japan), which was placed on a vibration

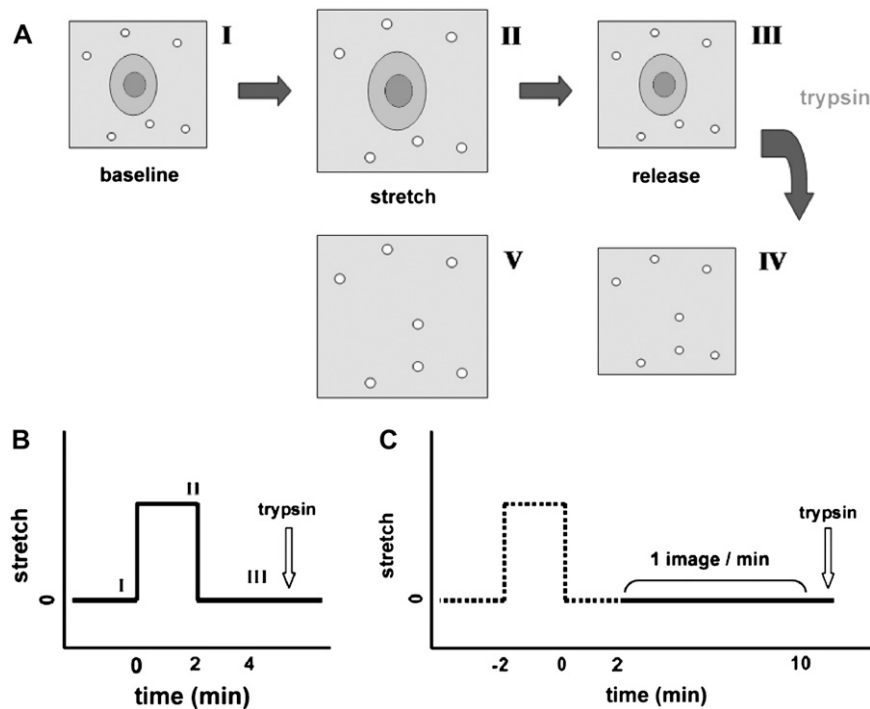


FIGURE 2 Experimental protocol. (A) Scheme of the traction microscopy protocol. A well containing a cell-cultured collagen gel was placed on the stretching device and bright field and fluorescence images of an isolated cell were acquired (I). The gel was stretched and bright field and fluorescence image acquisition was done again (II). The stretch was released and two final bright field and fluorescence images of the cell were acquired (III). After trypsin cell removal, a fluorescence reference image (RI) was recorded to assess the cell-free unstrained gel (IV). The gel was stretched again, and a fluorescence reference image was recorded to observe the cell-free strained gel (V). (B) Time course of the experimental protocol before cell detachment. (C) In traction recovery experiments, the protocol was extended to continue fluorescence image acquisition for 8 min (1 image/min) after stretch release.

isolation table (Isostation, Newport, Irvine, CA). All images were acquired with a 12-bit resolution cooled-CCD camera (Orca AG, Hamamatsu Photonics, Japan). For TM experiments, the apparent pixel size after magnification (20 \times) was 0.32 μm with a resulting field of view of $323 \times 323 \mu\text{m}^2$. The depth of focus of the objective was 2.7 μm , resulting in $\sim 10,000$ focused beads per fluorescence image. For actin staining experiments (10 \times), the depth of focus was 6.1 μm , enabling the recording of the entire fluorescence signal from a cell monolayer in one single image.

Data processing

Fluorescence images of the top of the gel were used to compute cell-induced and stretch-induced gel deformations. With this procedure, the fluorescent probes used to measure cell-matrix stresses were also used to compute the actual matrix strain in the region surrounding the cell with micrometer spatial resolution. To dissect gel deformations induced by cell traction forces from gel deformations exclusively due to substrate stretching, two different reference images (RIs) were obtained from the stretched and unstretched gels after detaching cells with trypsin (Fig. 2). To calculate stretch at the top of the gel due to substrate stretching, displacements of the fluorescent beads between the two RIs were first computed by image correlation (27) (see Fig. S2 in Data S1). Briefly, relative translational shift between the two images was first corrected by cross-correlation. Then, the images were iteratively divided into smaller windows and the displacement field between the two images was obtained by identifying the coordinates of the peak of the cross-correlation function between each pair of windows (27). Then, the stretch field ($S(x,y)$) was computed from the displacement field by using north and west gradient filters (see Fig. S2, B and C, in Data S1). A single representative stretch index (S) was then calculated as the median of pooled stretch data points.

To compute traction forces exerted by the cell on the substrate, the displacement field between each fluorescence image and the corresponding reference image (see Fig. S2 A in Data S1) was first computed using image correlation as described above. Simulations that used experimental values for the number of focused beads and the background noise showed that the signal/noise ratio (peak bead intensity divided by background noise) of the measured displacement field was ~ 50 . Traction force field ($T(x,y)$) was computed by common constrained Fourier transform traction cytometry

(CFTTC) algorithms (25), using E values of the corresponding stretch configuration. Cell area (A) and average cell traction (T) were computed as described elsewhere (28,32). An average of ~ 150 traction data points per cell was used to compute T .

For F-actin/G-actin fluorescence ratio quantification, background intensity for each image was calculated and subtracted. The sum of pixel intensities was computed for each F-actin and G-actin image, and the resultant values were used to calculate the ratio of fluorescence intensities (F/G actin) for each view (33). Five pairs of images were acquired for each well and averaged for a single data point. Positive controls of this technique in A549 cells are described elsewhere (28).

Statistics

Data are shown as mean \pm SE for $n = 6$ cells for each experiment. One-way analysis of variance was used to assess changes in E due to gel stretch. Two-way repeated measures one-way analysis of variance were used to analyze the effect of stretch in T and A . Comparison of baseline T between ML-7 pretreated and nonpretreated cells was carried out with an unpaired t -test. In stress recovery experiments, comparison of T between the initial and final time points was carried out with a paired t -test.

RESULTS

A new technique to map cell-matrix stresses during stretch

To assess changes in CSK tension during stretch we measured cell-matrix stresses exerted by adherent cells onto collagen gels with embedded submicron fluorescent beads. The relationship between the pressure applied under the flexible membrane and the resulting strain at the center of the upper gel surface was linear (see Fig. S3 in Data S1), thus enabling us to readily control cell stretch by adjusting the level of vacuum pressure. Although collagen gels subjected to large strain

exhibit nonaffine deformations, the network strain was fairly homogenous in the range of the macroscopic strain applied in this work ($<11\%$), with the distribution of local strain displaying a SD of $\sim 2.5\%$ (see Fig. S2, *E* and *F*, in [Data S1](#)). Most of this variability was accounted for by stretch-induced nonaffine deformations because variability in the stretch field arising from noise in the computed displacement field resulted in a SD of only $\sim 0.3\%$. In addition, the whole field of view of the surface of the gel remained in a common focus plane during stretch imposition, which discarded large local displacements of the beads in the z direction (see Fig. S1 in [Data S1](#)). Moreover, imposed macroscopic strain and resulting microscopic gel deformations were repeatable for successive stretching maneuvers and no residual strain was observed after stretch release. Additionally, the noise levels of the traction fields (measured by computing the traction stresses exerted by a cell-free gel region before and after stretch) were very small (see Fig. S2 *D* in [Data S1](#)).

As expected from the semiflexible nature of collagen fibers (17) the Young's modulus (E) of collagen gels displayed a strong dependence on applied strain (see Fig. S4 in [Data S1](#)). E of unstrained gels was 22.7 ± 5.5 Pa (mean \pm SD), whereas application of 5.5% and 11% strain increased E by twofold and 5.5-fold, respectively. The coefficient of variation (CoV = SD/mean) of E within samples was on average 52%. E was found to be similar over successive stretch applications of the same strain level (see Fig. S4 in [Data S1](#)).

Cell-matrix stresses increased with imposition of strain but dropped below baseline levels after stretch release

Under baseline conditions traction forces displayed a heterogeneous spatial distribution, with larger stresses mainly exerted along the cell periphery (Fig. 3). When the cell substrate was subjected to a 5.5% strain and maintained stretched, cell traction increased by 56% (Fig. 4). For a larger strain (11%), traction forces increased further (77%) but at a lower rate. When the cell substrate was relaxed to its initial conformation, traction forces were significantly lower than under baseline conditions. This drop in traction forces after stretch release increased markedly with the amplitude of the applied stretch. Cells did not show signs of rounding up or detachment after stretch, and cell spreading area A changed

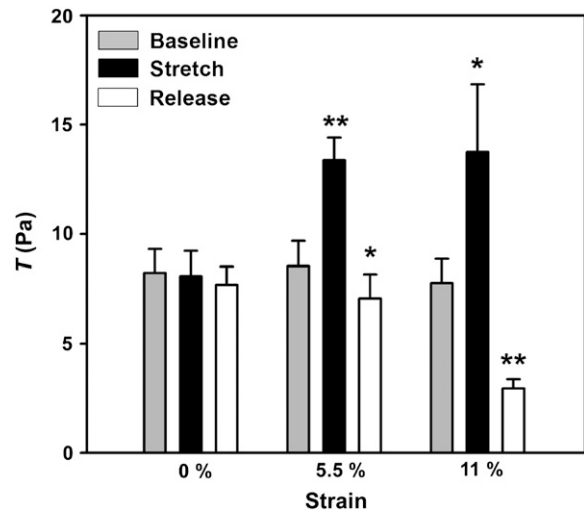


FIGURE 4 Effect of stretch on cell traction force. Average cell traction (T) measured before (baseline, gray bars), during (black bars) and after stretch release (white bars). Measurements were done at 0% strain (control), 5.5% strain, and 11% strain. Standard deviation of traction values within each cell was on average 3.6 Pa (42% CoV). Data are mean \pm SE ($n = 6$). * $p < 0.05$ and ** $p < 0.01$ versus baseline, respectively.

very little (4% decrease; see Fig. S6 in [Data S1](#)). This suggests that the reduction in traction observed after stretch release was not due to partial cell detachment but to a decrease in cell internal tension. To further analyze changes in cell stress after stretch release, we used stress maps to identify the sites of cell-matrix interaction that displayed larger drops in cell stress. Cell regions that exerted larger baseline traction forces also exhibited larger drops after stretch release with a relative drop roughly constant for all baseline traction force levels (Fig. 5). This decrease in traction forces was more marked at high levels of strain. To ascertain whether the changes in cell stress in response to stretch were caused by actin polymerization, we simultaneously stained F- and G-actin. No significant differences in F/G-actin fluorescence ratio were observed either during stretch or after release conditions (see Fig. S7 in [Data S1](#)).

In a second set of experiments, we studied the role of the actomyosin apparatus in the cell response to stretch by inhibiting MLCK with ML-7. Under these conditions, baseline traction forces were significantly lower than in control cells (Fig. 6). When the substrate was stretched, we found a relative

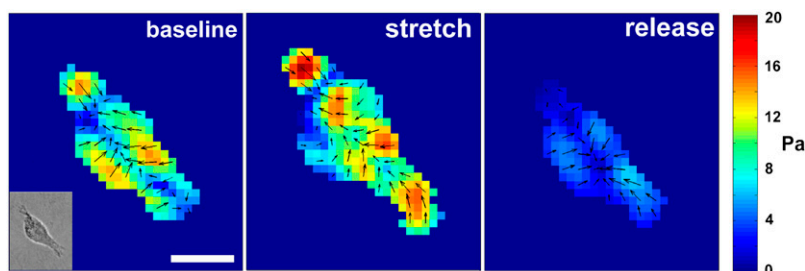


FIGURE 3 Effect of stretch on cell-matrix stresses. Traction fields exerted by an adhered cell in baseline (*left*), during stretch (11%) (*middle*) and after stretch release (*right*). Inset shows a bright field image of the cell in baseline. Color scale indicates the magnitude of traction forces and arrows depict the direction and relative magnitude of traction force. Traction forces were calculated with $2.6 \mu\text{m}$ spatial resolution. For clarity, arrows are displayed with $5.2 \mu\text{m}$ spacing. Scale bar is $20 \mu\text{m}$.

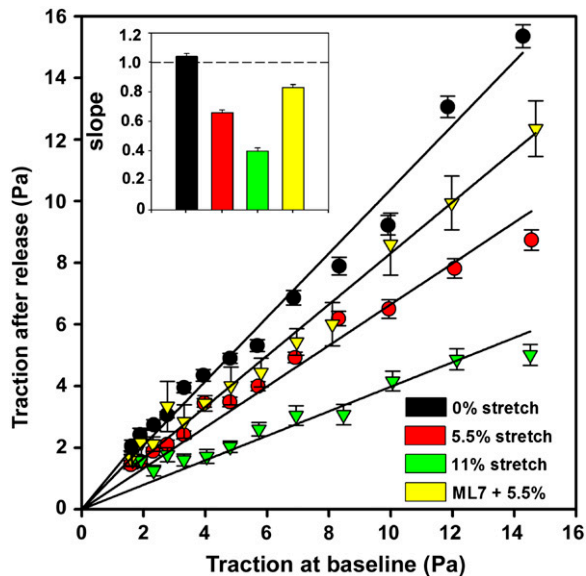


FIGURE 5 Dependence of local traction forces after stretch release on baseline traction. All data of traction fields of cells subjected to the same stretch level were pooled together and sorted by the magnitude of traction forces exerted under baseline conditions. The median of each group is plotted versus the median of the pooled traction forces in the same spatial points in stretch release configuration. Black circles correspond to cells subjected to no stretch (control), red circles to 5.5% stretch, green triangles to 11% stretch, and yellow triangles to cells pretreated with ML7 and subsequently subjected to 5.5% stretching. Traction forces below 1.5 Pa are not plotted because data were noisy. Data are mean \pm SE ($n = 6$). Lines are linear fits to the data. Inset: Values of the slopes obtained from linear fit of data in control (black bar), 5% stretch (red bar), 11% stretch (green bar), and ML7 + 5.5% stretch (yellow bar). Error bars are the standard error of the slopes provided by the fit ML7 + 5.5%. Dashed line corresponds to 1.

increase in traction forces larger than that of nonpretreated cells (Fig. 6, inset). After stretch release, we observed a nonsignificant drop in traction forces with respect to baseline conditions that was smaller than in nonpretreated cells. Regional distribution of traction forces was similar to nonpretreated conditions in baseline, stretch and release configurations (see Fig. S8 in Data S1). Regional changes in traction forces of ML7 pretreated cells showed a linear dependence on baseline traction force similar to that of nonpretreated cells (Fig. 5), but with a slope closer to one, indicating that the relaxation of CSK tension induced by a transient stretch is locally regulated by the prestress level.

We next studied the time course of cell-matrix stresses after stretch release. After a sudden drop, traction forces slowly recovered, reaching values close to baseline ~ 10 min after stretch release (Fig. 7 A and Movie S1). The analysis of dynamic stress maps (Fig. 7 B) showed that the regions with larger baseline traction forces displayed larger drops and slower traction force recovery after stretch release. By contrast, regions displaying smaller drops in traction forces exhibited a faster recovery, reaching traction forces that exceeded those under baseline conditions.

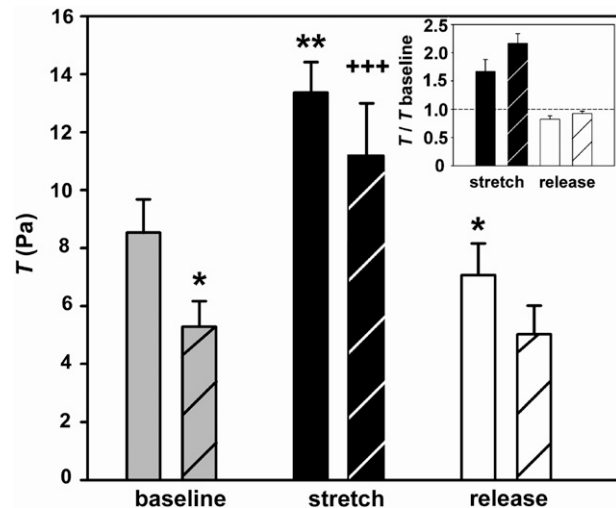


FIGURE 6 Effect of actomyosin inhibition on the cell stress response to stretch. Mean traction (T) of non-pretreated cells (solid bars) and cells pretreated with ML7 (dashed bars) and subsequently subjected to 5.5% strain. Gray bars correspond to baseline configuration, black bars to stretch configuration, and white bars to stretch release. Data are mean \pm SE ($n = 6$). * $p < 0.05$ and ** $p < 0.01$, respectively, versus baseline non-pretreated cells (solid gray bar). *** $p < 0.001$ versus baseline pretreated cells (dashed gray bar). (Inset) Ratio of T values under stretch or release conditions versus T under baseline conditions. Ratios were computed for each cell and then averaged. Solid bars indicate nonpretreated cells and dashed bars indicate cells pretreated with ML7. Dashed line corresponds to baseline.

DISCUSSION

Stretch imposition increases the amount of stresses exerted by adherent cells but stretch release results in drops of cell-matrix stresses below baseline levels. The relative increase in cell stress during stretch was found to be larger and the drop after stretch release was found to be smaller when the actomyosin machinery was inhibited. Cell-matrix stress maps showed that the loci of cell adhesion that initially bore greater stress also exhibited larger drops in cell-matrix stress after stretch removal. These sites of high baseline cell stress displayed poor recovery after the transient stretch, whereas rapid recovery took place at low baseline cell-matrix stress sites.

We implemented a novel technique to map cell-matrix stresses during application of stretch based on combining the traction microscopy technique (25,26) with equibiaxial substrate stretching (20). Unlike previous cell stretching devices (14,15) stretch was globally and equibiaxially applied, and the actual strain field of the cell substrate was measured for each sample with micrometer resolution. Our gels remained attached to the bottom and the walls of the well when stretch was applied to the lower surface of the gel. Therefore, the transmission of stretch from the elastic membrane to the upper surface of the gel does not depend on gel thickness or on its nonlinear elastic behavior. As a result, our setup exhibits a linear relationship between the stretch at the central region of the upper surface of the gel and the vacuum pressure applied underneath the elastic membrane (see Fig. S3 in

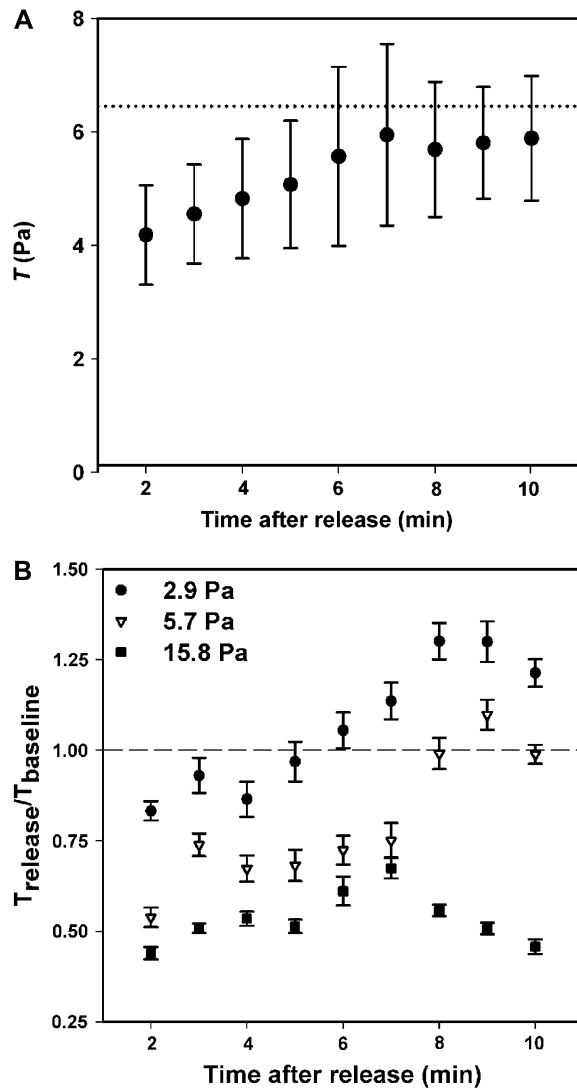


FIGURE 7 Cell-matrix stress recovery after stretch release. (A) Time course of traction force (T) recovery after stretch release of cells subjected to 5.5% strain. Data are mean \pm SE ($n = 6$). Time zero corresponds to stretch release. Dotted line is baseline T . (B) All data of traction fields were pooled together and sorted by the magnitude of traction forces exerted under baseline conditions. Time course recovery of each group is plotted as the median of the pooled traction forces after stretch release divided by the median of the same group under baseline conditions. Black circles correspond to points of the traction map initially exerting low tractions (1.5–4.5 Pa), white triangles to mid traction (4.6–9), and black squares to high traction (>9). Traction forces below 1.5 Pa are not plotted because data were noisy. Dashed line indicates the identity.

Data S1). It should be noted that substrate stretching resulted in lateral cell displacement and defocusing. As a consequence, traction microscopy measurements could not be done during the time required to reposition and refocus the sample (~ 2 min).

We used collagen type I gels as traction microscopy substrates because they firmly attached to the flexible-bottomed well and because they provide a much more physiological

environment to the cell than commonly used polyacrylamide gels or post arrays. Although collagen gels were less compliant than the extracellular matrix (34) and previously used traction microscopy gel substrates, we found no difference in cell shape or area between this work and a previous study carried out on the same cell type on stiffer polyacrylamide gels (28). In addition, we observed that cells cultured on collagen gels displayed common patterns of traction force distribution and responded to mechanical and biochemical stimuli (Figs. 4 and 6). The stiffness of collagen gels displayed a strong dependence on applied strain, which is consistent with previous reports for similar collagen concentration (17). The nonlinear elasticity of semiflexible biopolymer networks has been attributed to entropic elasticity due to a reduction of accessible thermal fluctuations of the filaments caused by the applied strain (16). Our collagen gels displayed a strain-hardening behavior similar to that exhibited by gels formed from cytoskeletal and extracellular proteins (17), thus reproducing the micromechanical environment experienced *in vivo* by cells subjected to stretch.

Our approach for the first time, to our knowledge, enables mapping of cell-matrix interactions during global and equibiaxial stretch application and after stretch removal. In addition, the actual strain field of the cell substrate was measured for each sample with micrometer resolution. Fluorescence images of the beads at the top of the gel were used to track both substrate-induced and cell-induced gel deformations. Our experimental approach was designed to make use of common TM algorithms to compute the traction field exerted by the cell onto the gel substrate. We applied the CFTTC algorithm developed by Butler and coworkers (25), which assumes that the net force applied to the substrate is zero. In our experimental setup, a comparison of fluorescence images acquired under stretch conditions versus a single RI acquired under nonstretch conditions would have given rise to a nonzero net force apparently exerted by the cell. This situation was avoided by acquiring two RIs, one on the nonstretch configuration and another on the stretch configuration. Nonzero net force can also arise when the lateral shift between fluorescence images is not corrected. In our experiments, stretch application resulted in large sample lateral shifts, which required a manual repositioning of the sample in the field of view of the microscope. Image overlap was improved during the data processing stage by applying 2D cross correlation to the whole images to accurately correct the translational shift between them. With this procedure, the displacement field only reflects the deformation induced by the cell, thereby fulfilling the zero net force assumption of the CFTTC algorithm. Therefore, the high spatial resolution of our experimental system allowed us to map tensional changes and spatial rearrangements taking place at the sites of cell-matrix attachment due to cell stretch.

Previous studies on the mechanical response of the adherent cell to stretch have shown that stretch increases cell stiffness (20,21,23), which is indicative of a nonlinear increase in CSK

tension with applied strain. The mechanism underlying such strain-stiffening remains in dispute but the analogous behavior exhibited by cross-linked actin networks suggests that entropic elasticity of single filaments is the main cause for nonlinear elasticity in the cell. Nevertheless, here we found that CSK tension increased when the cell was subjected to a small strain (5.5%) but the traction/stretch ratio was lower for larger strains (11%). On stretch release CSK tension dropped below baseline levels and recovered very slowly. Such responses cannot be explained solely by strain-hardening, reinforcement, or linear theories of viscoelasticity (6,24,35). Rather they suggest that stretch together with entropic strain-stiffening of single CSK filaments also induces inelastic rearrangements in the CSK lattice that lead to a drop in CSK tension.

The drop in CSK tension induced by a transient stretch could be explained by changes in actin polymerization, as has been shown to be the case in neutrophils entering narrow channels (36) or in adherent cells subjected to compressive stress (37). However, the finding that the F-actin to G-actin ratio is constant during the stretch-unstretch maneuver (see Fig. S7 in [Data S1](#)) argues against this possibility. In single cell TM experiments cell internal tension is balanced solely by the gel substrate via focal adhesion attachments. If some focal adhesions dissolved due to stretching, the distribution of traction forces could be modified but the total traction exerted by the gel through the remaining attachments to balance a given CSK tension would not change. In addition, as shown in Fig. 5, all the loci of cell attachment underwent similar relative decreases in traction forces after stretch release. Therefore, the drop in cell traction induced by a transient stretch does not seem to be attributable to rearrangements of cell-substrate attachments. An alternative mechanism could be that filament cross-links and actomyosin cross-bridges are not able to withstand the increase in tension of the CSK lattice caused by stretch and they are therefore forced to rupture or unfold (23,24,38). This interpretation is supported by our finding that when lowering the tension of the CSK by partially inhibiting myosin activity, the relative increase in cell stress with stretch was larger than that in control samples and the drop in stress after the transient stretch was substantially attenuated. Moreover, we have reported recently in the same cell type that reducing actomyosin activation by inhibiting MLC-kinase or Rho-kinase pathways does not modify the regional distribution of traction forces (28). This suggests that, under relaxed conditions with low levels of CSK tension, semiflexible CSK filaments are able to deform in response to stretch by pulling out their thermal fluctuations. By contrast, when myosin motors tense actin filaments increasing CSK tension, the CSK lattice becomes increasingly uncompliant, forcing cross-bridges and cross-links to yield to accommodate the imposed deformation. Our findings suggest that the increase in cell traction induced by stretching is due to a rise in the passive elastic recoil of the distended CSK network, which is partially counterbalanced by a fall in active contractile tension caused by stretch-induced acto-

myosin detachment. It has been suggested that only excessive cell distension may detach actin myosin cross links, thus causing actively generated internal tension to dissipate (23). By contrast, comparison of our cell-matrix stress maps before and after stretch showed that for all levels of strain actively generated tension exerted at the sites of cell adhesions decreased (Fig. 5). Furthermore, the adhesions that initially withstood larger stresses were those that showed the largest drop after stretch release. This indicates that the regions of the CSK subjected to larger initial tension are those that yield more easily when the cell is stretched.

Maps of cell-matrix stresses show that the rate of stress recovery after stretch is not spatially homogeneous. Rather, cell stresses are dramatically redistributed after stretch. Moreover, tension recovery seems to be attributed to the structures less affected by stretch, whereas the regions subjected to the largest stress drop display little recovery (Fig. 7 B). Interestingly, a recent study showed an opposite relationship between the global rate of stiffness recovery after stretch and the baseline level of tension (24). This apparent discrepancy suggests that cells exhibit a different mechanical behavior at the local level and at the global level.

Cell prestress is believed to be a key parameter in determining cell mechanical behavior and mechanotransduction processes. It determines the rheology of the cytoskeleton and its rate of remodeling (24,39). In addition, changes in cell prestress resulting from external stress application provide a mechanism to sense mechanical cues and locally trigger signaling cascades (40). Cell prestress is commonly thought to provide a protective mechanism by which the cell can preserve its shape and structural integrity in response to external stresses; the larger the applied stress; the larger the cell resistance to deform (6,10). Here we show this view to be largely incomplete. When the cell is forced to undergo a given strain, regardless of the applied stress, the role of prestress is reversed and the larger the prestress, the closer the CSK is to yield. In this case, prestress does not protect the structural integrity of the CSK but rather it brings it closer to rupture when a mechanical deformation is externally applied. Our results suggest that this is because cytoskeletal structures subjected to tension break in response to strain. Such disruption is not catastrophic, however, and it provides a new mechanism that the cell uses to rapidly remodel its CSK and adapt to a dynamic environment without using chemical energy.

SUPPLEMENTARY MATERIAL

To view all of the supplemental files associated with this article, visit www.biophysj.org.

The authors are indebted to M. Rodríguez for technical assistance and B. Fabry for helpful suggestions.

This work was supported in part by Ministerio de Educación y Ciencia (NAN2004-09348-C04-04, SAF2005-00110) and Ministerio de Sanidad y Consumo (FIS-PI040929).

REFERENCES

1. Chicurel, M. E., C. S. Chen, and D. E. Ingber. 1998. Cellular control lies in the balance of forces. *Curr. Opin. Cell Biol.* 10:232–239.
2. Janmey, P. A. 1998. The cytoskeleton and cell signaling: component localization and mechanical coupling. *Physiol. Rev.* 78:763–781.
3. Huang, S., and D. E. Ingber. 1999. The structural and mechanical complexity of cell-growth control. *Nat. Cell Biol.* 1:E131–E138.
4. Ingber, D. E. 2006. Cellular mechanotransduction: putting all the pieces together again. *FASEB J.* 20:811–827.
5. Vogel, V., and M. P. Sheetz. 2006. Local force and geometry sensing regulate cell functions. *Nat. Rev. Mol. Cell Biol.* 7:265–275.
6. Ingber, D. E. 2003. Tensegrity I. Cell structure and hierarchical systems biology. *J. Cell Sci.* 116:1157–1173.
7. Bausch, A. R., and K. Kroy. 2006. A bottom-up approach to cell mechanics. *Nat. Phys.* 2:231–238.
8. An, S. S., R. E. Laudadio, J. Lai, R. A. Rogers, and J. J. Fredberg. 2002. Stiffness changes in cultured airway smooth muscle cells. *Am. J. Physiol. Cell Physiol.* 283:C792–C801.
9. Sylvester, J. T. 2004. The tone of pulmonary smooth muscle: ROK and Rho music? *Am. J. Physiol. Lung Cell. Mol. Physiol.* 287:L624–L630.
10. Wang, N., J. P. Butler, and D. E. Ingber. 1993. Mechanotransduction across the cell surface and through the cytoskeleton. *Science.* 260:1124–1127.
11. Rivelino, D., E. Zamir, N. Q. Balaban, U. S. Schwarz, T. Ishizaki, S. Narumiya, Z. Kam, B. Geiger, and A. D. Bershadsky. 2001. Focal contacts as mechanosensors: externally applied local mechanical force induces growth of focal contacts by an mDia1-dependent and ROCK-independent mechanism. *J. Cell Biol.* 153:1175–1186.
12. Yoshigi, M., E. B. Clark, and H. J. Yost. 2003. Quantification of stretch-induced cytoskeletal remodeling in vascular endothelial cells by image processing. *Cytometry A.* 55:109–118.
13. Mack, P. J., M. R. Kaazempur-Mofrad, H. Karcher, R. T. Lee, and R. D. Kamm. 2004. Force-induced focal adhesion translocation: effects of force amplitude and frequency. *Am. J. Physiol. Cell Physiol.* 287:C954–C962.
14. Munevar, S., Y. L. Wang, and M. Dembo. 2004. Regulation of mechanical interactions between fibroblasts and the substratum by stretch-activated Ca^{2+} entry. *J. Cell Sci.* 117:85–92.
15. Sniadecki, N. J., A. Anguelouch, M. T. Yang, C. M. Lamb, Z. Liu, S. B. Kirschner, Y. Liu, D. H. Reich, and C. S. Chen. 2007. Magnetic microposts as an approach to apply forces to living cells. *Proc. Natl. Acad. Sci. USA.* 104:14553–14558.
16. Gardel, M. L., J. H. Shin, F. C. MacKintosh, L. Mahadevan, P. Matsudaira, and D. A. Weitz. 2004. Elastic behavior of cross-linked and bundled actin networks. *Science.* 304:1301–1305.
17. Storm, C., J. J. Pastore, F. C. MacKintosh, T. C. Lubensky, and P. A. Janmey. 2005. Nonlinear elasticity in biological gels. *Nature.* 435:191–194.
18. Gardel, M. L., F. Nakamura, J. H. Hartwig, J. C. Crocker, T. P. Stossel, and D. A. Weitz. 2006. Prestressed F-actin networks cross-linked by hinged filamins replicate mechanical properties of cells. *Proc. Natl. Acad. Sci. USA.* 103:1762–1767.
19. Pourati, J., A. Maniotis, D. Spiegel, J. L. Schaffer, J. P. Butler, J. J. Fredberg, D. E. Ingber, D. Stamenovic, and N. Wang. 1998. Is cytoskeletal tension a major determinant of cell deformability in adherent endothelial cells? *Am. J. Physiol.* 274:C1283–C1289.
20. Trepatt, X., M. Grabulosa, F. Puig, G. N. Maksym, D. Navajas, and R. Farre. 2004. Viscoelasticity of human alveolar epithelial cells subjected to stretch. *Am. J. Physiol. Lung Cell. Mol. Physiol.* 287:L1025–L1034.
21. Fernandez, P., P. A. Pullarkat, and A. Ott. 2006. A master relation defines the nonlinear viscoelasticity of single fibroblasts. *Biophys. J.* 90:3796–3805.
22. Matthews, B. D., D. R. Overby, R. Mannix, and D. E. Ingber. 2006. Cellular adaptation to mechanical stress: role of integrins, Rho, cytoskeletal tension and mechanosensitive ion channels. *J. Cell Sci.* 119:508–518.
23. Rosenblatt, N., S. Hu, B. Suki, N. Wang, and D. Stamenovic. 2007. Contributions of the active and passive components of the cytoskeletal prestress to stiffening of airway smooth muscle cells. *Ann. Biomed. Eng.* 35:224–234.
24. Trepatt, X., L. Deng, S. S. An, D. Navajas, D. J. Tschumperlin, W. T. Gerthoffer, J. P. Butler, and J. J. Fredberg. 2007. Universal physical responses to stretch in the living cell. *Nature.* 447:592–595.
25. Butler, J. P., I. M. Tolic-Norrelykke, B. Fabry, and J. J. Fredberg. 2002. Traction fields, moments, and strain energy that cells exert on their surroundings. *Am. J. Physiol. Cell Physiol.* 282:C595–C605.
26. Dembo, M., and Y. L. Wang. 1999. Stresses at the cell-to-substrate interface during locomotion of fibroblasts. *Biophys. J.* 76:2307–2316.
27. Tolic-Norrelykke, I. M., J. P. Butler, J. Chen, and N. Wang. 2002. Spatial and temporal traction response in human airway smooth muscle cells. *Am. J. Physiol. Cell Physiol.* 283:C1254–C1266.
28. Gavara, N., R. Sunyer, P. Roca-Cusachs, R. Farre, M. Rotger, and D. Navajas. 2006. Thrombin-induced contraction in alveolar epithelial cells probed by traction microscopy. *J. Appl. Physiol.* 101:512–520.
29. Alcaraz, J., L. Buscemi, M. Grabulosa, X. Trepatt, B. Fabry, R. Farre, and D. Navajas. 2003. Microrheology of human lung epithelial cells measured by atomic force microscopy. *Biophys. J.* 84:2071–2079.
30. Burnham, N. A., X. Chen, C. S. Hodges, G. A. Matei, E. J. Thoreson, C. J. Roberts, M. C. Davis, and S. J. B. Tendler. 2003. Comparison of calibration methods for atomic-force microscopy cantilevers. *Nanotechnology.* 14:1–6.
31. Rico, F., P. Roca-Cusachs, N. Gavara, R. Farre, M. Rotger, and D. Navajas. 2005. Probing mechanical properties of living cells by atomic force microscopy with blunted pyramidal cantilever tips. *Phys. Rev. E Stat. Nonlin. Soft Matter Phys.* 72:021914.
32. Marganski, W. A., V. M. De Biase, M. L. Burgess, and M. Dembo. 2003. Demonstration of altered fibroblast contractile activity in hypertensive heart disease. *Cardiovasc. Res.* 60:547–556.
33. Hirshman, C. A., H. Togashi, D. Shao, and C. W. Emala. 1998. Gi-2 is required for carbachol-induced stress fiber formation in human airway smooth muscle cells. *Am. J. Physiol. Lung Cell. Mol. Physiol.* 275:L911–L916.
34. Yuan, H., S. Kononov, F. S. Cavalcante, K. R. Lutchen, E. P. Ingenito, and B. Suki. 2000. Effects of collagenase and elastase on the mechanical properties of lung tissue strips. *J. Appl. Physiol.* 89:3–14.
35. Sheetz, M. P. 2001. Cell control by membrane-cytoskeleton adhesion. *Nat. Rev. Mol. Cell Biol.* 2:392–396.
36. Yap, B., and R. D. Kamm. 2005. Cytoskeletal remodeling and cellular activation during deformation of neutrophils into narrow channels. *J. Appl. Physiol.* 99:2323–2330.
37. Costa, K. D., W. J. Hucker, and F. C. Yin. 2002. Buckling of actin stress fibers: a new wrinkle in the cytoskeletal tapestry. *Cell Motil. Cytoskeleton.* 52:266–274.
38. Trepatt, X., F. Puig, N. Gavara, J. J. Fredberg, R. Farre, and D. Navajas. 2006. Effect of stretch on structural integrity and micromechanics of human alveolar epithelial cell monolayers exposed to thrombin. *Am. J. Physiol. Lung Cell. Mol. Physiol.* 290:L1104–L1110.
39. Wang, N., I. M. Tolic-Norrelykke, J. Chen, S. M. Mijailovich, J. P. Butler, J. J. Fredberg, and D. Stamenovic. 2002. Cell prestress. I. Stiffness and prestress are closely associated in adherent contractile cells. *Am. J. Physiol. Cell Physiol.* 282:C606–C616.
40. Sawada, Y., M. Tamada, B. J. Dubin-Thaler, O. Cherniavskaya, R. Sakai, S. Tanaka, and M. P. Sheetz. 2006. Force sensing by mechanical extension of the Src family kinase substrate p130Cas. *Cell.* 127:1015–1026.